Applied Catalysis B: Environmental 101 (2011) 382–387

Contents lists available at ScienceDirect

Applied Catalysis B: Environmental

journal homepage: www.elsevier.com/locate/apcatb

Significantly enhanced photocatalytic performance of ZnO via graphene hybridization and the mechanism study

Tongguang Xu[1], Liwu Zhang[1], Hanyun Cheng, Yongfa Zhu*

Department of Chemistry, Tsinghua University, Beijing 100084, PR China

ARTICLE INFO

Article history:
Received 26 July 2010
Received in revised form
30 September 2010
Accepted 5 October 2010
Available online 14 October 2010

Keywords:
Graphene
Photocatalysis
ZnO
Photoelectrochemical

ABSTRACT

Graphene hybridized with ZnO could produce an efficient photocatalyst. The ZnO nanoparticles were firstly coated with an appropriate amount of graphene oxide, the graphene oxide was then in situ reduced to form the ZnO/graphene composite. Graphene hybridized ZnO photocatalyst showed enhanced photocatalytic activity for the degradation of organic dye. The degree of photocatalytic activity enhancement strongly depended on the coverage of graphene on the surface of ZnO nanoparticles. The sample of 2 wt% graphene hybridized ZnO showed the highest photocatalytic activity, which was about 4 times as that of pristine ZnO. The enhancement of photocatalytic activity was attributed to the high migration efficiency of photo-induced electrons and the inhibited charge carriers recombination due to the electronic interaction between ZnO and graphene. The electronic interaction was systematically studied and confirmed by the photoelectrochemical measurements.

1. Introduction

Heterogeneous photocatalysts offer great potential for environmental purification and converting photon energy into chemical energy [1,2]. A major limitation to achieve high photocatalytic efficiency is the quick recombination of photo-generated charge carries. Recombination has faster kinetics than surface redox reactions and greatly reduces the quantum efficiency of photocatalysis. Therefore, to enhance the photocatalysis efficiency, it is essential to retard the recombination of the charge carriers. Many works have been devoted to reduce the recombination of charge carriers by coupling the photocatalysts with other materials, such as noble metals [3,4], semiconductors [5,6], carbon nanotube [7], etc. Our group has developed conjugative π structure material hybridized semiconductor as efficient photocatalysts, such as C_{60} [8,9], polyaniline [10,11], graphite-like carbon [12,13]. Graphene as a two-dimensional macromolecular sheet of carbon atoms has superior electrical conductivity and mechanical properties [14,15], which would make it an excellent electron-transport material in the process of photocatalysis, even more appropriate than C_{60}, polyaniline, graphite-like carbon. It is expected that the hybridization of photocatalyst with graphene would reduce the recombination of charge carriers, and increase the photocatalytic efficiency. Recently, some efforts have been made to utilize the unique properties of graphene to increase the efficiency of photocatalysis [16–22], and to increase the efficiency of solar cells [23–25]. However, the interior mechanism and some details are yet not very clear: the optimal amount of graphene on the surface of photocatalyst, the chemical and electronic interaction at the interface of graphene and photocatalyst, and the active species during the graphene modified photocatalysis, etc. Systematical study on a purpose of understanding the interaction between graphene and photocatalysts and further effect on the photocatalytical activity is still necessary and important.

Several methods have been reported to synthesize metal oxide-graphene composites (such as TiO_2, Al_2O_3, and SnO_2, etc.) [19,26–28]. Herein, different amount of graphene was loaded on the surface of photocatalyst particles to form the photocatalyst/graphene composite. To obtain ZnO/graphene composite with intimate contact at the interface, ZnO nanoparticles were firstly coated with an appropriate amount of graphene oxide, the graphene oxide was then in situ chemically reduced to form the ZnO/graphene composite with hydrazine. By this method, ZnO nanoparticles could efficiently separate the graphene sheets and retard the restacking of the graphene sheets during graphene oxide reduction. We chose ZnO as a model active photocatalyst, some studies have confirmed that ZnO exhibits a better efficiency than TiO_2 in photocatalytic degradation of some dyes [29,30]. In the present work, we report an efficient photocatalyst by loading graphene on the surface of ZnO. Enormous enhancement of photocatalytic efficiency was observed by surface modification of ZnO with graphene. The structure and interface electronic interaction between ZnO and graphene, as well as the resulting effect on the photocatalytic activity were systematically investigated.

* Corresponding author. Tel.: +86 10 62783586; fax: +86 10 62787601.
E-mail address: zhuyf@tsinghua.edu.cn (Y. Zhu).
[1] This two authors contribute equally to this work.

0926-3373/$ – see front matter © 2010 Elsevier B.V. All rights reserved.
doi:10.1016/j.apcatb.2010.10.007

2. Experimental

2.1. Materials preparation

Graphene oxide (GO) was prepared from natural graphite by the reported method [26,31]. Particulate ZnO (particle diameter 10–20 nm, surface area 57.3 $m^2\ g^{-1}$) were commercially available. All chemicals used were reagent grade without further purification. Graphene hybridized ZnO sample was prepared as follows: Appropriate as-prepared graphite oxide was dispersed in water to create a 0.05 wt% dispersion. Exfoliation of graphite oxide to GO was achieved by ultrasonication of the dispersion for 30 min. The obtained brown dispersion was then subjected to 30 min of centrifugation at 3000 rpm to remove any unexfoliated graphite oxide. The obtained exfoliated graphite oxide was then dispersed in 50 mL water, and 1 g ZnO was added into the GO dispersion. Then ZnO and GO mixture was dispersed by ultrasonication for 30 min and stirred for 24 h. The reduction of GO to graphene is performed according to literature [3]. In a typical procedure, appropriate amount of hydrazine solution (35 wt% in water) and ammonia solution (28 wt% in water) were added to the above dispersion. The weight ratio of hydrazine to GO was about 7:10. After being vigorously shaken or stirred for a few minutes, the dispersion was put in a water bath (95 °C) for 1 h. An opaque powder was obtained after evaporated at 80 °C for 10 h.

2.2. Characterization

High resolution transmission electron microscopy (HRTEM) images were obtained by JEM 2010F field emission transmission electron microscope with an accelerating voltage of 200 kV. The diffuse reflectance absorption spectra (DRS) of the samples were recorded on a UV–vis spectrophotometer (Hitachi UV-3100) equipped with an integrated sphere attachment, and the spectra were recorded in the range of 200–800 nm. Raman spectra were recorded on a microscopic confocal Raman spectrometer (Renishaw 1000 NR) with an excitation of 514.5 nm laser light. Electrochemical and photoelectrochemical measurements were performed in a home made three electrode quartz cells. Pt sheet was used as counter and Hg/Hg_2Cl_2/sat. KCl used as reference electrodes, while the working electrode was the thin film on indium-tin oxide (ITO) for investigation. The photoelectrochemical experiment results were recorded with a CHI 660B electrochemical system. The electron spin resonance (ESR) signals of radicals spin-trapped by spin-trap reagent 5,5′-dimethyl-1-pirroline-N-oxide (DMPO) (purchased from Sigma Chemical Co.) were examined on a Bruker model ESR 300E spectrometer equipped with a quanta-Ray Nd:YAG laser system as the irradiation source (λ = 355 nm, 10 Hz). The settings for the ESR spectrometer were as follows: center field, 3486.70 G; sweep width, 100 G; microwave frequency, 9.82 GHz; modulation frequency, 100 kHz; power, 5.05 mW. To minimize experimental errors, the same quartz capillary tube was used for all ESR measurements. The ESR spectrometer was coupled to a computer for data acquisition and instrument control. Magnetic parameters of the radicals detected were obtained from direct measurements of magnetic field and microwave frequency.

2.3. Photochemical experiments

The photocatalytic activities of the as-prepared samples for the degradation of methylene blue (MB) in solution were tested under UV light. An 8 W UV lamp (λ = 254 nm,) was used as light resource, and the average light intensity was 0.95 mW/cm^2. 50 mg of graphene hybridized ZnO photocatalysts was dispersed in a 100 mL MB suspension (1×10^{-5} M). Prior to the irradiation, the suspensions were magnetically stirred in the dark for 30 min to reach the absorption–desorption equilibrium. At given time intervals, 3 mL of the aliquots were sampled and analyzed by recording variations in the absorption band (665 nm) in the UV–vis spectra of MB using a Hitachi U-3010 UV–vis spectrophotometer.

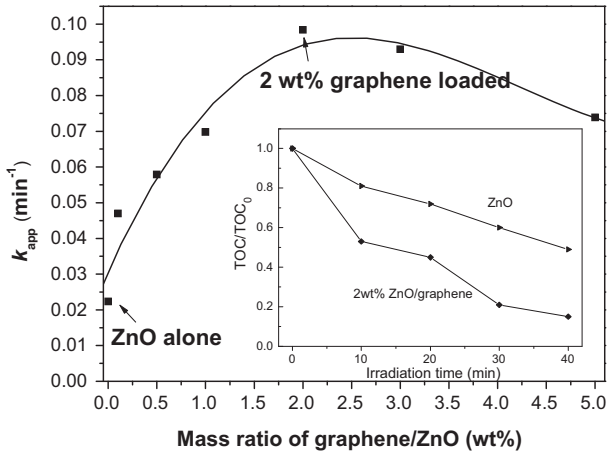

Fig. 1. The effect of the graphene loading on the apparent rate constant (k) of MB photodegradation. Catalyst loading, 50 mg; MB, 10^{-5} M, 100 mL; average light intensity, 0.95 mW/cm^2. Inset: Total organic carbon removal on ZnO and ZnO/graphene composite.

ZnO/graphene and ZnO electrodes were prepared by a dip-coating method: 5 mg of photocatalyst was suspended in 5 mL ethanol to make a slurry, the slurry was then dip-coated onto a 2 cm × 4 cm indium-tin oxide glass electrode. The electrodes were then exposed to UV light for 12 h to eliminate ethanol, and calcined at 200 °C for 30 min in flowing N_2 with a rate of 60 mL min^{-1}. A saturated calomel electrode (SCE), and a Pt gauze was immersed in the reactor as reference, and counter electrodes. Prior to and during all measurements, the electrolyte (0.5 M Na_2SO_4) was purged with nitrogen. All investigated electrodes show a similar thickness (0.8–1 μm).

3. Results and discussion

3.1. Enhancement of photocatalytic activity

Photocatalytic experiments were carried out by degradation of methyl blue (MB) under UV light. Fig. 1 shows the photodegradation rates of MB on ZnO/graphene catalysts with different loading amounts of graphene. One can see that all the ZnO/graphene samples exhibit much higher photocatalytic activities than the pure ZnO sample. Pure ZnO presents an apparent reaction rate constant k of 0.022 min^{-1}, while the sample of ZnO hybridized with 0.1 wt% of graphene shows an apparent reaction rate constant of 0.047 min^{-1}, which is more than twice faster than ZnO alone. The sample with 2.0 wt% of graphene showed the highest activity (k = 0.098 min^{-1}), the activity of MB degradation was increased by more than 3 times after 2.0 wt% of graphene loaded. The total organic carbon (TOC) is also measured (see inset of Fig. 1), it is found that the TOC removal percentage is 80% and less than 40% for ZnO/graphene (2.0 wt%) and ZnO after 30 min photocatalytic reaction. When the loading amount was below 2.0 wt%, the photocatalytic activities enhanced with the increased loading amount of graphene, however, when the loading amount exceeded 2.0 wt%, the photocatalytic activities of samples decreased as the amount of graphene increased. The optimal loading amount of graphene on the surface of ZnO nanoparticles was 2.0 wt%. The decreased activity at higher graphene loading is attributed to increased absorbance and scattering of photons through excess graphene in the photosystem.

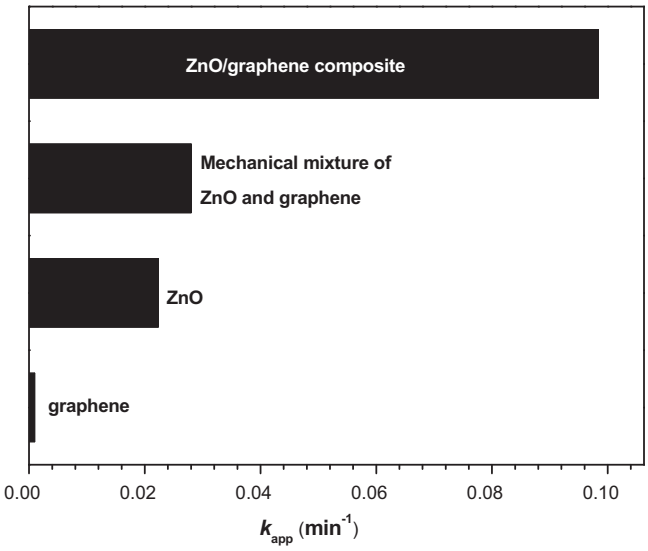

Fig. 2. The apparent rate constant of MB photodegradation on graphene, ZnO, mechanical mixture of ZnO and graphene (2.0 wt%), and the ZnO/graphene (graphene 2.0 wt%) composite. Catalyst loading, 50 mg; MB, 10^{-5} M, 100 mL; average light intensity, 0.95 mW/cm^2.

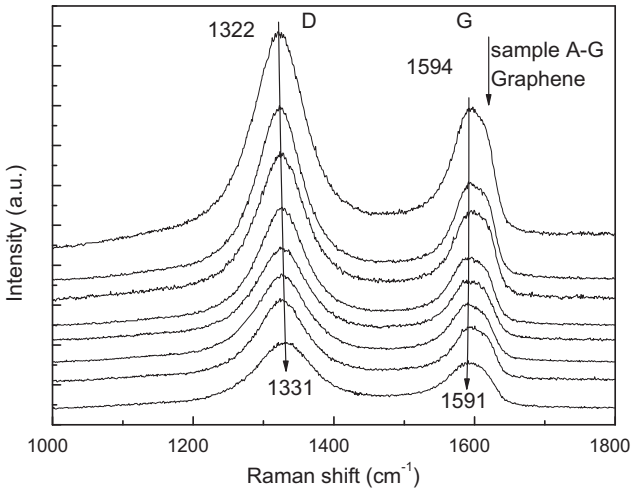

Fig. 3. Raman spectra of graphene and ZnO/graphene composites. Samples A–G represent ZnO/graphene composites with 5.0 wt%, 3.0 wt%, 2.0 wt%, 1.0 wt%, 0.5 wt%, 0.2 wt%, and 0.1 wt% of graphene loaded, respectively.

Fig. 2 shows the photodegradation rates of MB on graphene, ZnO, ZnO/graphene composite, and mechanical mixture of ZnO and graphene. Graphene shows negligible photodegradation of MB. The mechanical mixture of ZnO and graphene (2 wt%) shows slightly higher photocatalytic activity than that of pure ZnO, while the ZnO/graphene composite with the same amount of graphene loading possesses a much higher activity. The four times higher activity of ZnO/graphene composite compared with mechanical mixture of ZnO and graphene is attributed to the intimate contact between ZnO and graphene, which is crucial for the formation of electronic interaction and interelectron transfer at the interface.

3.2. Hybrid structure and optical properties

UV–vis spectrum (see supporting information Fig. S1) of the as-prepared graphene dispersion showed an absorption peak at 275 nm with a broad absorption background that is consistent with that of reported aqueous stable graphene sheets [31]. Herein, the ZnO nanoparticles were firstly coated with an appropriate amount of graphene oxide, then, the graphene oxide was in situ reduced by hydrazine hydrate to form the ZnO/graphene composite. The ZnO/graphene samples were characterized by Raman spectra (Fig. 3). The Raman spectra of graphene and ZnO/graphene composite showed similar G and D bands structure of carbon, suggesting that the structure of graphene is maintained in the composite of ZnO/graphene. All samples exhibit two peaks around 1325 and 1590 cm^{-1}. The Raman-active E_{2g} mode at 1590 cm^{-1}, characteristic of the presence of sp^2 carbon-type structures present within the ZnO/graphene samples. The D band at around 1325 cm^{-1} is associated with the presence of defects in the hexagonal graphitic layers. It is notable that the Raman peaks of graphene shift gradually as the mass ratio of graphene and ZnO varies. Compared with pristine graphene, the D band was slightly blue-shifted by 9 cm^{-1} in the ZnO/graphene composites, while the G band showed a red-shift of 3 cm^{-1}. These shifts in the Raman peak could be attributed to the chemical interaction between ZnO and graphene.

The hybridization structure of ZnO and graphene is further investigated by HRTEM. The 2D graphene sheets and ZnO nanoparticles are clearly observed from Fig. 4A. The graphene sheets are not perfectly flat but display intrinsic microscopic roughening and out of plane deformations (wrinkles). The HRTEM image in Fig. 4B

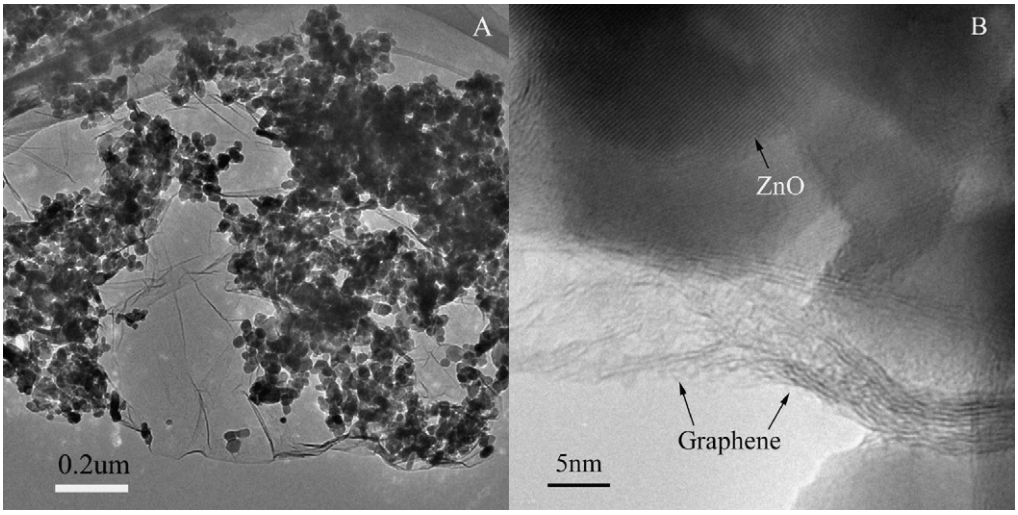

Fig. 4. TEM (A) and HRTEM (B) images of ZnO/graphene composite (2.0 wt %).

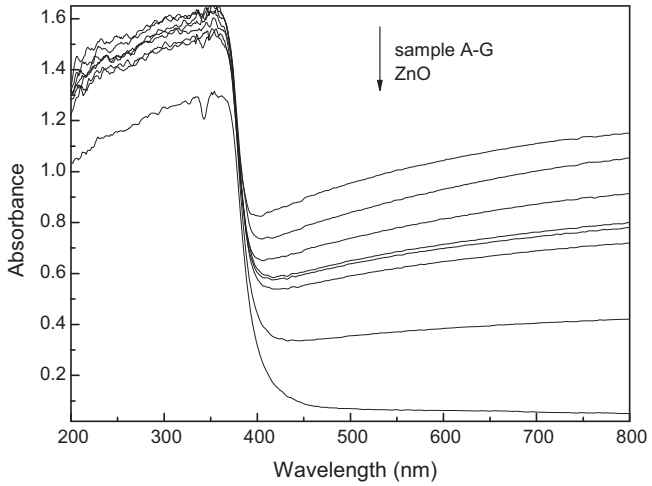

Fig. 5. UV–vis diffuse reflection spectra of ZnO and ZnO/graphene samples. Samples A–G represent ZnO/graphene composites with 5.0 wt%, 3.0 wt%, 2.0 wt%, 1.0 wt%, 0.5 wt%, 0.2 wt%, and 0.1 wt% of graphene loaded, respectively.

shows the intimate contact between ZnO and graphene. This intimate contact makes possible the electronic interaction between ZnO and graphene, and improves the charge separation and the photocatalytic activity.

The optical properties of ZnO/graphene samples were probed by UV–vis diffuse reflectance spectroscopy, as shown in Fig. 5. As expected, ZnO shows the characteristic spectrum with its fundamental absorption sharp edge rising at 400 nm, while the ZnO/graphene samples absorb in the whole visible region due to the presence of graphene on ZnO. The absorption edge of ZnO can also be detected in ZnO/graphene samples. With the loading of graphene, The ZnO/graphene samples displayed the same absorption edge as that of ZnO. In present work, the carbon in ZnO/graphene samples was free graphitic carbon. Therefore, the band gap energy was not changed, and an intense, broad background absorption in visible region was observed in UV–vis spectra. In addition, it is noticeable that there is an obvious correlation between the carbon content and the UV–vis spectrum change. The enhancements of absorption increase with graphene contents of the ZnO/graphene samples. These observations might suggest an increase of surface electric charge of the oxides in the composite due to graphene introduction, which may lead to modifications of the fundamental process of electron/hole pair formation while irradiation.

3.3. Photoelectric properties

Photoelectrochemical experiments were then performed to investigate the electronic interaction between ZnO and graphene. Fig. 6 displays the photocurrent transient responses for ZnO and ZnO/graphene electrodes. It is clear that fast and uniform photocurrent responses were observed for each switch-on and switch-off event in both electrodes. The photocurrent transients have almost the same shape for each electrode. When the illumination is stopped, the photocurrent decreases back to zero. It is worthy to note that the photocurrent of the ZnO/graphene electrode is about 3.5 times as high as that of the ZnO electrode. The photocurrent enhancement of graphene hybridized ZnO indicated a higher separation efficiency of photo-induced electrons and holes, which could be attributed to the interaction of graphene and ZnO semiconductor. The ability of electron transfer from excited semiconductor to the graphene sheet has been detected by time-resolved fluorescence spectroscopy in the CdS/graphene nanocomposite [32]. Mott–Sckottky (MS) measurements were performed in darkness

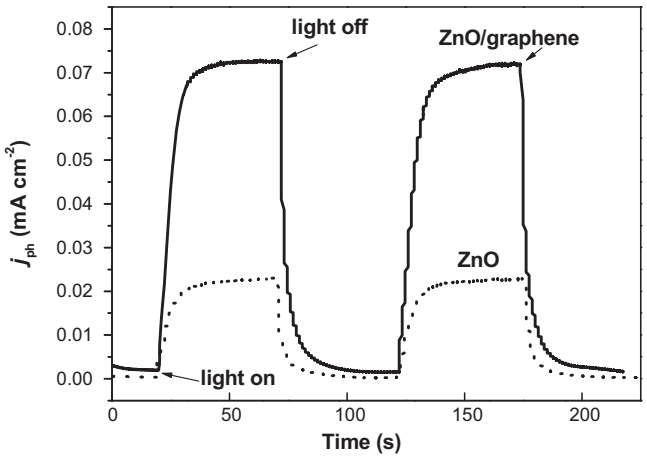

Fig. 6. Photocurrent transient responses of ZnO and ZnO/graphene electrodes. [Na_2SO_4] = 0.5 M.

by using the impedance technique. Fig. 7 shows the MS plots of the electrodes based on sintered ZnO and ZnO/graphene. Reversed sigmoidal plots were observed with an overall shape consistent with that typical for n-type semiconductors. The flat-band potential could be obtained from the *x* intercepts of the linear region, which were found at −0.36 and −0.29 V for ZnO and ZnO/graphene, respectively. The ZnO/graphene electrode showed a positive shift of the flat-band potential as compared with the ZnO electrode. In addition, the slope of the linear region for the ZnO/graphene electrode showed a lower value, clearly indicating higher donor density for ZnO/graphene electrode.

The electrochemical impedance spectroscopy (EIS) responses also indicate that more effective separation of photo-generated electron–hole pairs and faster interfacial charge-transfer occurred in the case of graphene hybridized ZnO electrode (see supporting information Fig. S2). Fig. S2 shows the electrochemical EIS Nynquist plots of ZnO and ZnO/graphene electrodes before and after UV irradiation. In each case, only one arc/semicircle on the EIS plane could be observed, suggesting that only the surface charge-transfer step is in the photocatalytic reaction. The radius of the arc on the EIS Nynquist plots reflects the reaction rate occurring at the surface of the electrode. The arc radius on the EIS Nynquist plot of ZnO/graphene electrode was much smaller than that of ZnO electrode, indicating a fast interfacial charge-transfer to the electrode donor/electron acceptor and an effective

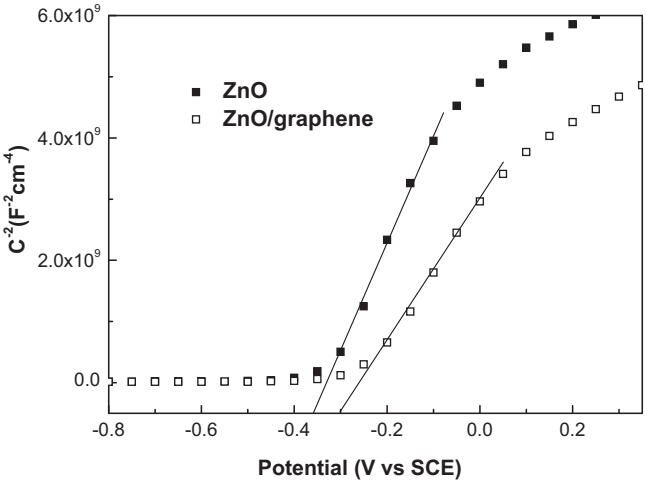

Fig. 7. Mott–Schottky plots of ZnO and ZnO/graphene electrodes.

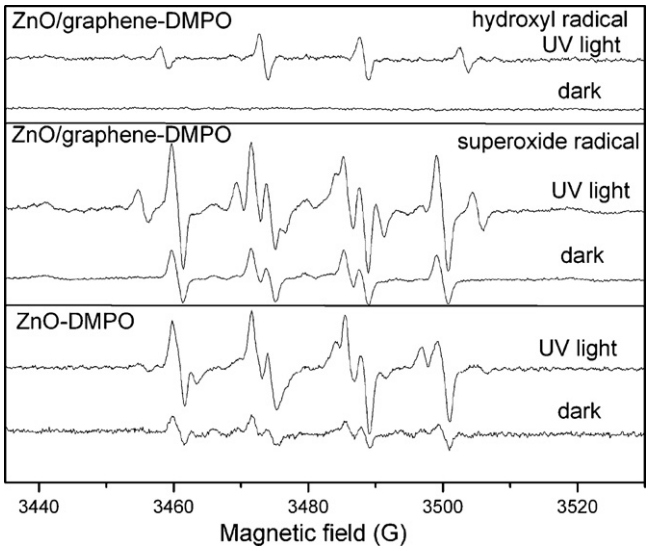

Fig. 8. DMPO spin-trapping ESR spectra ZnO and ZnO/graphene.

separation of photo-generated electron–hole pairs as suggested [33,34].

3.4. Photocatalytic mechanism

The photocatalytic mechanism was studied by ESR (electron spin resonance) spin-trap technique and trapping experiments of radicals and holes. ESR spin-trap technique (with DMPO) was employed to monitor the reactive oxygen species generated during the irradiation of the present system, the result was shown in Fig. 8. Both the signals of DMPO—•OH and DMPO—$O_2^{\bullet-}$ could be clearly observed when prestine ZnO and graphene hybridized ZnO suspension were irradiated by a Quanta-Ray Nd:YAG pulsed laser system (λ = 355 nm, 10 Hz). Therefore, a dual mechanism involving both hydroxyl radicals and $O_2^{\bullet-}$ radicals oxidation is expected in the photocatalysis process. Fig. 9 shows the photodegradation of MB with the addition of holes and hydroxyl radicals scavengers, respectively. The addition of 1 mM tert-butanol as hydroxyl radicals scavenger caused a decrease of the photocatalytic degradation of MB, while the MB could be hardly degraded with the addition of capture for holes (EDTA-Na), suggesting that the free hydroxyle radicals were not the main active oxidative species in the photocatalytic degradation of MB, but direct hole oxidation and $O_2^{\bullet-}$ oxidation reaction mainly govern the photocatalytic process.

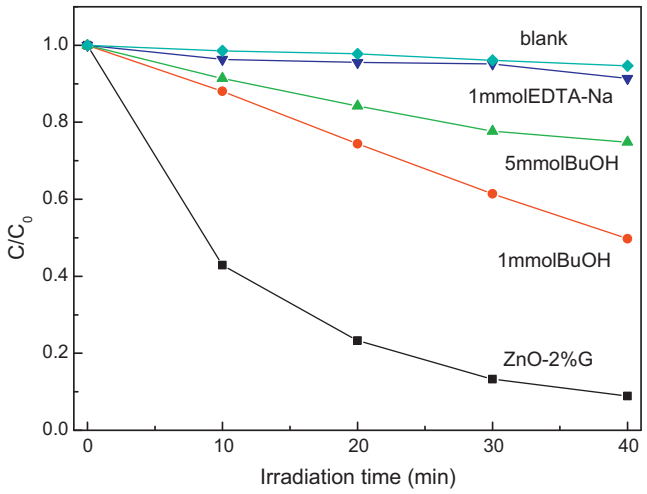

Fig. 9. Photocatalytic degradation of MB with the additon of hole and radical scavenger.

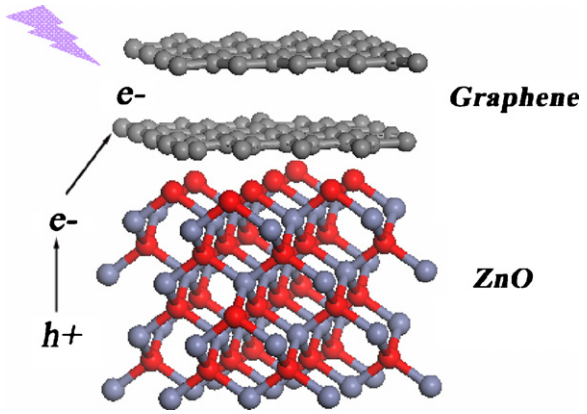

Scheme 1. Schematic drawing of ZnO/graphene composite under UV light irradiation.

The much higher photocatalytic activity of graphene hybridized ZnO than the mechanical mixture of ZnO and graphene indicated that the electronic interaction between ZnO and graphene is crucial, which could significantly increase the separation of photo-generated charge. The enhancement of photocatalytic activity of ZnO after graphene hybridization could be attributed to the higher separation efficiency of electron–hole pairs caused by the rapid photo-induced charge separation and the inhibition of the recombination of electron–hole pairs, resulting in the increase of the number of holes participated in the photooxidation process. In the present work, graphene mainly existed on the surface of ZnO. Graphene, with delocalized conjugated π structure and superior electrical conductivity, could efficient transfer the photo-generated electrons. Thus, the possibility of the recombination of e^-/h^+ pairs decrease. The photo-generated electrons in the ZnO/graphene photocatalyst could easily migrate for the inner region to the surface to take part in the surface reaction to form radicals such as $O_2^{\bullet-}$ by reacting with O_2 absorbed on the surface. The enhancement of charge carrier separation would result in more reactive oxygen species (such as •OH, $O_2^{\bullet-}$), the increment of the amount of reactive species is confirmed by ESR (electron spin resonance) spin-trap experiments (Fig. S4). The schematic illustration of the mechanism of the enhancement of photocatalytic activity is summarized in Scheme 1.

The stability of ZnO/graphene as photocatalyst was also studied. The photocatalytic activity did not decrease after five successive cycles of degradation tests, indicating that the composite is fairly stable under the studied conditions.

In summary, we have demonstrated that the hybridization with graphene on the surface of ZnO could significantly increase the photocatalytic efficiency of ZnO. The activity is increased by almost five times when loaded with 2.0 wt% graphene. The electronic interaction between graphene and ZnO is supposed to be responsible for the enhanced photocatalytic activity and photocurrent conversion. Further works that hybridize graphene with other photocatalysts are underway.

Acknowledgments

This work was partly supported by Chinese National Science Foundation (20925725 and 20673065) and National Basic Research Program of China (2007CB613303). L.Z. acknowledges the Alexander von Humboldt (AvH) Foundation for granting him a research fellowship.

Appendix A. Supplementary data

Supplementary data associated with this article can be found, in the online version, at doi:10.1016/j.apcatb.2010.10.007.

References

[1] M.R. Hoffmann, S.T. Martin, W. Choi, D.W. Bahnemann, Chem. Rev. 95 (1995) 69.
[2] D. Ravelli, D. Dondi, M. Fagnoni, A. Albini, Chem. Soc. Rev. 38 (2009) 1999–2011.
[3] T. Hirakawa, P.V. Kamat, J. Am. Chem. Soc. 127 (2005) 3928–3934.
[4] V. Subramanian, E.E. Wolf, P.V. Kamat, J. Am. Chem. Soc. 126 (2004) 4943–4950.
[5] S.H. Elder, F.M. Cot, Y. Su, S.M. Heald, A.M. Tyryshkin, M.K. Bowman, Y. Gao, A.G. Joly, M.L. Balmer, A.C. Kolwaite, K.A. Magrini, D.M. Blake, J. Am. Chem. Soc. 122 (2000) 5138–5146.
[6] T. Tatsuma, S. Saitoh, P. Ngaotrakanwiwat, Y. Ohko, A. Fujishima, Langmuir 18 (2002) 7777–7779.
[7] K. Woan, G. Pyrgiotakis, W. Sigmund, Adv. Mater. 21 (2009) 2233–2239.
[8] H.B. Fu, T.G. Xu, S.B. Zhu, Y.F. Zhu, Environ. Sci. Technol. 42 (2008) 8064–8069.
[9] S.B. Zhu, T.G. Xu, H.B. Fu, J.C. Zhao, Y.F. Zhu, Environ. Sci. Technol. 41 (2007) 6234–6239.
[10] H. Zhang, R.L. Zong, Y.F. Zhu, J. Phys. Chem. C 113 (2009) 4605–4611.
[11] H. Zhang, R.L. Zong, J.C. Zhao, Y.F. Zhu, Environ. Sci. Technol. 42 (2008) 3803–3807.
[12] L.W. Zhang, H.Y. Cheng, R.L. Zong, Y.F. Zhu, J. Phys. Chem. C 113 (2009) 2368–2374.
[13] L.W. Zhang, H.B. Fu, Y.F. Zhu, Adv. Funct. Mater. 18 (2008) 2180–2189.
[14] C. Berger, Z. Song, X. Li, X. Wu, N. Brown, C. Naud, D. Mayou, T. Li, J. Hass, A.N. Marchenkov, E.H. Conrad, P.N. First, W.A. de Heer, Science 312 (2006) 1191–1196.
[15] S. Stankovich, D.A. Dikin, G.H.B. Dommett, K.M. Kohlhaas, E.J. Zimney, E.A. Stach, R.D. Piner, S.T. Nguyen, R.S. Ruoff, Nature 442 (2006) 282–286.
[16] H. Zhang, X. Lv, Y. Li, Y. Wang, J. Li, ACS Nano 4 (2009) 380–386.
[17] J.L. Wu, X.P. Shen, L. Jiang, K. Wang, K.M. Chen, Appl. Surf. Sci. 256 (2010) 2826–2830.
[18] X.Y. Zhang, H.P. Li, X.L. Cui, Y.H. Lin, J. Mater. Chem. 20 (2010) 2801–2806.
[19] G. Williams, B. Seger, P.V. Kamat, Acs Nano 2 (2008) 1487–1491.
[20] G. Williams, P.V. Kamat, Langmuir 25 (2009) 13869–13873.
[21] T.N. Lambert, C.A. Chavez, B. Hernandez-Sanchez, P. Lu, N.S. Bell, A. Ambrosini, T. Friedman, T.J. Boyle, D.R. Wheeler, D.L. Huber, J. Phys. Chem. C 113 (2009) 19812–19823.
[22] O. Akhavan, E. Ghaderi, J. Phys. Chem. C 113 (2009) 20214–20220.
[23] N.L. Yang, J. Zhai, D. Wang, Y.S. Chen, L. Jiang, Acs Nano 4 (2010) 887–894.
[24] S.R. Kim, M.K. Parvez, M. Chhowalla, Chem. Phys. Lett. 483 (2009) 124–127.
[25] Y.B. Tang, C.S. Lee, J. Xu, Z.T. Liu, Z.H. Chen, Z.B. He, Y.L. Cao, G.D. Yuan, H.S. Song, L.M. Chen, L.B. Luo, H.M. Cheng, W.J. Zhang, I. Bello, S.T. Lee, Acs Nano 4 (2010) 3482–3488.
[26] D. Wang, D. Choi, J. Li, Z. Yang, Z. Nie, R. Kou, D. Hu, C. Wang, L.V. Saraf, J. Zhang, I.A. Aksay, J. Liu, ACS Nano 3 (2009) 907–914.
[27] X. Wang, S.M. Tabakman, H. Dai, J. Am. Chem. Soc. 130 (2008) 8152–8153.
[28] C. Nethravathi, J.T. Rajamathi, N. Ravishankar, C. Shivakumara, M. Rajamathi, Langmuir 24 (2008) 8240–8244.
[29] K. Gouvea, F. Wypych, S.G. Moraes, N. Duran, N. Nagata, P. Peralta-Zamora, Chemosphere 40 (2000) 433.
[30] S. Dindar, J. Icli, J. Photochem. Photobiol. A: Chem. 140 (2001) 263.
[31] D. Li, M.B. Muller, S. Gilje, R.B. Kaner, G.G. Wallace, Nat. Nanotechnol. 3 (2008) 101–105.
[32] A. Cao, Z. Liu, S. Chu, M. Wu, Z. Ye, Z. Cai, Y. Chang, S. Wang, Q. Gong, Y. Liu, Adv. Mater. 21 (2009).
[33] W.H. Leng, Z. Zhang, J.Q. Zhang, C.N. Cao, J. Phys. Chem. B 109 (2005) 15008–15023.
[34] L.W. Zhang, Y.J. Wang, H.Y. Cheng, W.Q. Yao, Y.F. Zhu, Adv. Mater. 21 (2009) 1286–1290.